ISSN 0036-0295, Russian Metallurgy (Metally), Vol. 2016, No. 9, pp. 826–831. © Pleiades Publishing, Ltd., 2016.
Original Russian Text © E.N. Sheftel', E.V. Kharin, V.A. Tedzhetov, G.Sh. Usmanova, A.I. Krikunov, 2016, published in Metally, 2016, No. 5, pp. 54–60.

Magnetic Anisotropy Induced in the Nanocrystalline FeZrN Films Prepared by Oblique-Angle Magnetron Sputtering

E. N. Sheftel'[a, *], E. V. Kharin[a], V. A. Tedzhetov[a], G. Sh. Usmanova[a], and A. I. Krikunov[b]

[a] *Baikov Institute of Metallurgy and Materials Science, Russian Academy of Sciences, Leninskii pr. 49, Moscow, 119334 Russia*

[b] *OOO Fotron-Avto, Moscow, Russia*

**e-mail: sheftel@imet.ac.ru*

Received January 12, 2016

Abstract—Nanocrystalline $Fe_{77}Zr_7N_{16}$ films are prepared by oblique-angle magnetron sputtering. The effect of the ion beam angle and subsequent annealing on the phase and structural states, the coercive force, the saturation magnetization, the remanent magnetization, and the induced in-plane magnetic anisotropy field has been studied. The possibility of natural ferromagnetic resonance in these films at gigahertz frequencies is estimated.

DOI: 10.1134/S0036029516090147

INTRODUCTION

The modern progress trends in microelectronics include the creation of miniature high-frequency induction electronic devices operating at gigahertz frequencies. Such devices are used in radio engineering (microinductor, microtransformers), for data storage (magnetic recording heads), and so on. Soft magnetic film materials intended for magnetic cores of the aforementioned devices should be characterized by a high saturation induction (B_s) and magnetic permeability (μ) at gigahertz frequencies. Natural ferromagnetic resonance frequency ${}_e f_{FMR}$, which determines the upper limit of ac field frequency (in this field, magnetic permeability μ is high), can be shifted to a high-frequency range in films characterized by high saturation magnetization (M_s) and in-plane magnetic anisotropy field (H_k) [1–3]; ${}_e f_{FMR} = \gamma(4\pi M_s H_k)^{1/2}$ ($\gamma =$ 2.8 MHz/80 A/m). It is known that in-plane magnetic anisotropy can be induced, in particular, during so-called oblique-angle deposition, during which an ion beam falls at a certain angle to a substrate and the film growing on it [4–6].

Earlier, we showed that the Fe$M_{IV}X$ films (M_{IV} = IVA Group metals of the periodic table and X = N, C, B) prepared by reactive magnetron sputtering can assure a unique combination of properties, which includes a saturation induction of $B_s = \sim 2$ T, a coercive force of $H_c < 80$ A/m, a local (within grain) anisotropy field of $H_a < 80$ kA/m, and thermal stability up to 600°C. Scarce data on the high-frequency application of film materials of this class are available. Taking into account the prospects of a high magnetic permeability to be reached in Fe–$M_{IV}X$ films at gigahertz frequencies, in the present study we investigate the effect of the oblique angle of the incident ion beam on in-plane induced magnetic anisotropy field H_k, the phase and structural states, and the static magnetic properties of $Fe_{77}Zr_7N_{16}$ films classified among the aforementioned film materials.

EXPERIMENTAL

We studied $Fe_{77}Zr_7N_{16}$ films prepared from an $Fe_{95}Zr_5$ target by high-frequency reactive oblique-angle magnetron sputtering. The films were deposited on amorphous SiO_2 or multilayer $Si/SiO_2/Si_3N_4$ substrates used in microelectronics (multilayer substrates consist of Si single crystal having the [001] orientation, amorphous SiO_2 layer 0.4 μm thick, and top Si_3N_4 layer 0.16 μm thick). $Fe_{77}Zr_7N_{16}$ films 0.5 μm thick were prepared by magnetron sputtering at oblique angles of incident ion beam α = 0°, 10°, 20°, and 30° (relative to the normal to the substrate plane). The film thickness was determined using an interference microscope. The preparation conditions of the $Fe_{77}Zr_7N_{16}$ films are characterized by the following magnetron sputtering parameters:

Magnetron power, W	300
Residual atmospheric pressure, Pa	665×10^{-6}
Working gas pressure, Pa	465.5×10^{-3}
Working gas composition	Ar + 10% N_2
Target-to-substrate distance, mm	50
Sputtering time, min	16

The sputtered films were annealed in a vacuum of 133×10^{-6} Pa at temperatures of 400 and 500°C for 1 h

(at these annealing temperatures, films having close compositions exhibited the best combination of B_s and H_c [7–9]). The heating rate during annealing was 2 K/min and the cooling rate was no more than 10 K/min.

The chemical composition of the films was determined in a vacuum of 133×10^{-5} Pa using a Quanta 200 scanning electron microscope equipped with an EDXRMA energy dispersive X-ray analyzer. Deviations of the zirconium and nitrogen contents from those corresponding to the average composition $Fe_{77}Zr_7N_{16}$ were no more than 1 at % for all films.

The phase composition and the bstructure of the films were studied by X-ray diffraction (XRD). Full-profile X-ray diffraction patterns were taken in a 2θ angular range of 5°–105° at a step of 0.05° and 3-s exposure per point using a DRON-3 diffractometer, a graphite monochromator, and Cu$K\alpha$ radiation. The initial processing of X-ray diffraction patterns was performed using the OUTSET software [10]. A qualitative phase analysis was carried out using the database of Joint Committee on Powder Diffraction Standards and the PHAN program. A quantitative analysis and the calculations of grain size $2R_c$ and root-mean square microstrain ε (described by Gaussian) were performed with the Rietveld method and the PHAN% program. Lattice parameter a was calculated using the OUTSET software.

The magnetic properties of the films were measured on a vibrating-sample magnetometer at room temperature in a magnetic field up to 560 kA/m. Magnetic anisotropy K_u induced by oblique-angle sputtering was determined as the area between the hysteresis loops measured along the easy and hard magnetization directions (shaded area in Fig. 1).

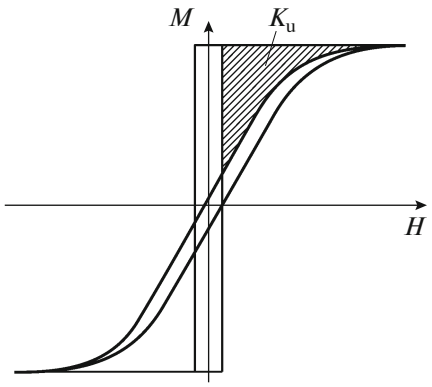

Fig. 1. Schematic hysteresis loops measured along the easy (square) and hard (sloped) magnetization directions. Shaded area corresponds to induced magnetic anisotropy K_u.

RESULTS AND DISCUSSION

Phase and Structural States of the Films

XRD results are given in Table 1 and Fig. 2. The X-ray diffraction patterns of as-sputtered films deposited on SiO_2 substrates are characterized by a broad

Table 1. Results of processing of the X-ray diffraction patterns of the $Fe_{77}Zr_7N_{16}$ films (phase composition corresponds to 100 vol % α-Fe)

α, deg	a, Å	$2R_c$, nm	ε, %
1. As-sputtered films (SiO_2 substrate)			
0	2.942 ± 0.004	2.3	0.100
10	2.935 ± 0.003	3.0	0.100
20	2.930 ± 0.003	2.1	0.100
30	2.921 ± 0.001	4.0	0.100
Annealing at 400°C for 1 h (SiO_2 substrate)			
0	2.887 ± 0.001	5.2	0.010
10	2.895 ± 0.001	3.0	0.100
20	2.902 ± 0.001	2.1	0.100
30	2.896 ± 0.001	4.0	0.100
Annealing at 500°C for 1 h (SiO_2 substrate)			
10	2.885 ± 0.003	5.2	0.115
20	2.878 ± 0.001	7.1	0.436
2. As-sputtered films ($Si/SiO_2/Si_3N_4$ substrate)			
0	2.942 + 0.002	2.3	0.100
10	2.925 ± 0.001	3.2	0.100
20	2.930 ± 0.002	2.5	0.100
30	2.925 ± 0.001	3.3	0.100
Annealing at 500°C for 1 h ($Si/SiO_2/Si_3N_4$ substrate)			
20	2.864 ± 0.001	23.2	0.018
30	2.885 ± 0.001	11.0	0.771

a is the lattice parameter, $2R_c$ is the grain size, and ε is the root-mean-square microstrain (described by Gaussian).

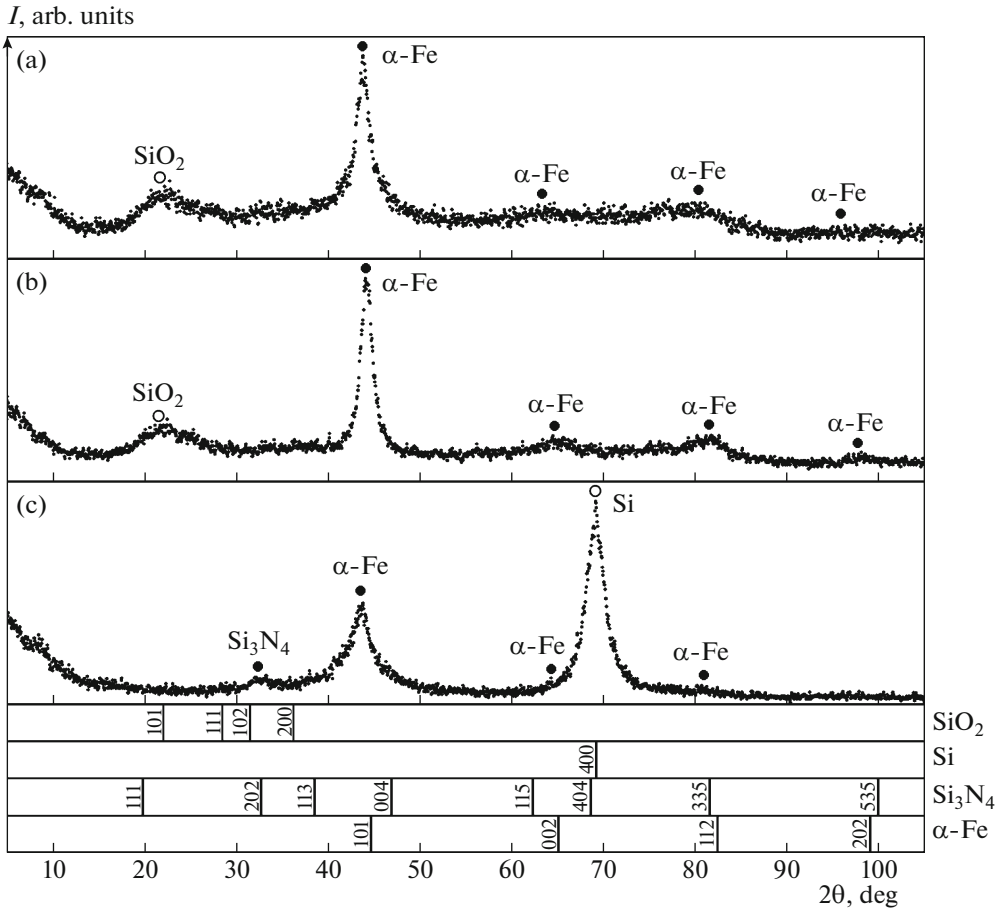

Fig. 2. X-ray diffraction patterns for (a, c) as-sputtered and (b) annealed at 400°C films sputtered on (a, b) SiO_2 and (c) $Si/SiO_2/Si_2N_4$ substrates at oblique angles of (c) 0° and (a, b) 30°. Bar diagrams of the found phases are given at the bottom.

(110) reflection of the bcc α-Fe-based phase. The lattice parameter of the phase varies from 2.942 to 2.921 Å depending on the deposition angle. The lattice parameter is substantially higher than that of unalloyed α-Fe in a nanocrystalline film (2.824 ± 0.003 Å) [9] and the polycrystalline bulk material (2.866 Å). This is related to the formation of a supersaturated nitrogen and zirconium solution in α-Fe during deposition.

In the range of low angles, the X-ray diffraction patterns exhibit a reflection related to the amorphous substrate; the center of gravity of the reflection corresponds to $2\theta \approx 22°$ (see Fig. 2). Its appearance is related to the fact that the depth of X-ray penetration exceeds the film thickness.

Since the second-order (211) reflection of the bcc phase in the films cannot be determined to an acceptable accuracy, grain size $2R_c$ and grain microstrain ε were determined using the (110) reflection of the bcc phase and the procedure described in [11]. The average grain size of the bcc phase varies within a range of 2–4 nm and the root-mean-square microstrain (described by Gaussian) is ~0.1%.

The X-ray diffraction pattern of the films deposited on $Si/SiO_2/Si_3N_4$ substrates (Fig. 2c) exhibits the reflections of the nanocrystalline bcc α-Fe-based phase and the reflections related to the substrate materials (Si, Si_3N_4). In this case, the bcc phase is the nitrogen and zirconium solid solution in α-Fe with an average grain size of 2–3 nm and a root-mean-square microstrain of ~0.1%. The formation of the solid solution is indicated by a substantially higher lattice parameter (from 2.942 to 2.925 Å depending on the oblique angle) as compared to that of microcrystalline α-Fe (2.866 Å).

The annealing of the films deposited on SiO_2 substrates decreases the lattice parameter of the bcc phase, because nitrogen and zirconium atoms leave the solid solution, and slightly increases the grain size of the phase to 5–7 nm (Fig. 3).

Effect of the Ion Beam Angle

For all the as-sputtered films, whatever the substrate composition, the lattice parameter of the bcc phase decreases with increasing oblique angle (see

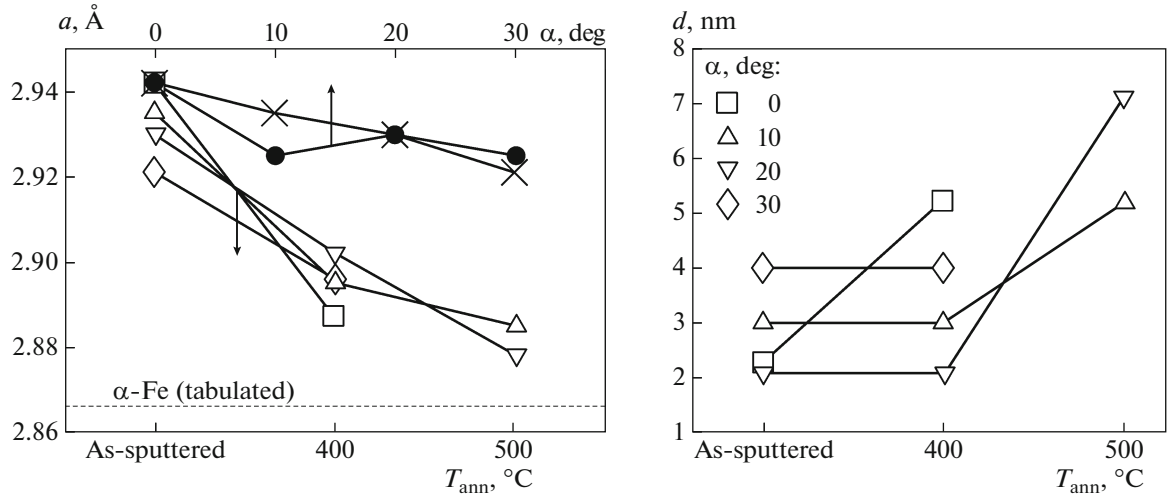

Fig. 3. (a) Lattice parameter a and (b) grain size d of the bcc α-Fe-based phase in the as-sputtered films prepared at oblique angles (□) 0°, (△) 10°, (▽) 20°, and (◇) 30° and annealed at 400 and 500°C. (a) Lattice parameter a of the bcc α-Fe phase in the as-sputtered and annealed films deposited on (×) SiO_2 and (●) $Si/SiO_2/Si_3N_4$ substrate at different oblique angles.

Table 1, Fig. 3). This is explained as follows. In the case of normal ion-beam incidence on the substrate surface, a film grows along the beam incidence direction. During oblique-angle ion-beam incidence, the interaction between the normal component of the beam and the growing film becomes weaker, whereas the tangent component enhances with increasing slope of the ion beam. In this case, energy, in particular, temperature conditions of the film growth change [12]; this can lead to structural changes similar to those observed during annealing. However, as is seen from Fig. 3 and Table 1, the annealings lead to a more substantial decrease in the lattice parameter of the bcc phase as compared to that observed when the slope of the ion beam increases.

Static Magnetic Properties

Table 2 and Figs. 4a and 4b show the results of measuring coercive force H_c, relative remanent magnetization M_r/M_s, saturation magnetization M_s, and induced magnetic anisotropy field $H_k = 2K_u/M_s$ of the $Fe_{77}Zr_7N_{16}$ films.

As the oblique angle increases, the induced anisotropy field (H_k) and coercive force (H_c) of as-sputtered films increase (see Fig. 4), whereas the relative remanent magnetization (M_r/M_s) decreases. The existence of extended portion of hysteresis loop in fields above the coercive force, which is observed for the as-sputtered films (Fig. 5a), indicates the presence of perpendicular anisotropy in them. Such an anisotropy is

Table 2. Coercive force H_c, relative remanent magnetization M_r/M_s, and saturation magnetization M_s of the $Fe_{77}Zr_7N_{16}$ films sputtered at several oblique angles α and annealed at various temperatures T_{ann}

T_{ann}, °C	α, deg	Substrate	M_s, G	M_r/M_s	H_c, A/m
Without HT	0	$Si/SiO_2/Si_3N_4$	1398 ± 13	0.45	696 ± 16
	10		1051 ± 6	0.28	1520
	20		1428 ± 10	0.32	960
	30		1126 ± 8	0.18	1040 ± 240
400	0	SiO_z	455 ± 3	0.58	480 ± 240
	10		677 ± 6	0.50	480 ± 320
	20		934 ± 9	0.20	128 ± 8
	30		704 ± 3	0.22	72 ± 56
500	10	SiO_2	1053 ± 4	0.13	320 ± 160
	20		890 ± 3	0.08	56 ± 8
	20	$Si/SiO_2/Si_3N_4$	711 ± 5	0.04	32 ± 16
	30		933 ± 3	0.03	24 ± 16

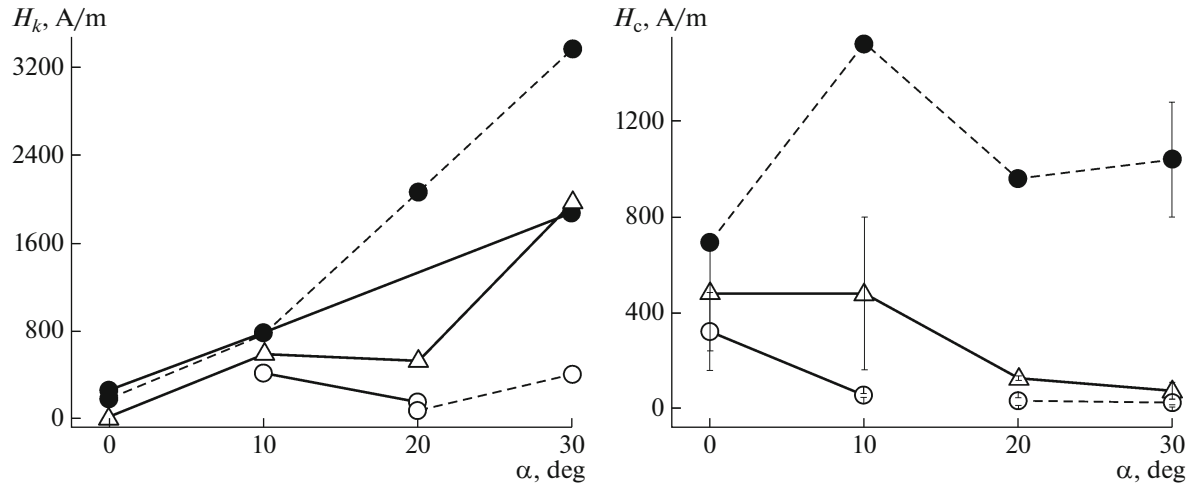

Fig. 4. Induced anisotropy field H_k and coercive force H_c of the $Fe_{77}Zr_7N_{16}$ (●) as-sputtered films prepared at different oblique angles and the films annealed at (△) 400 and (○) 500°C. Solid and dashed lined correspond to the films deposited on SiO_2 and $Si/SiO_2/Si_3N_4$ substrates, respectively.

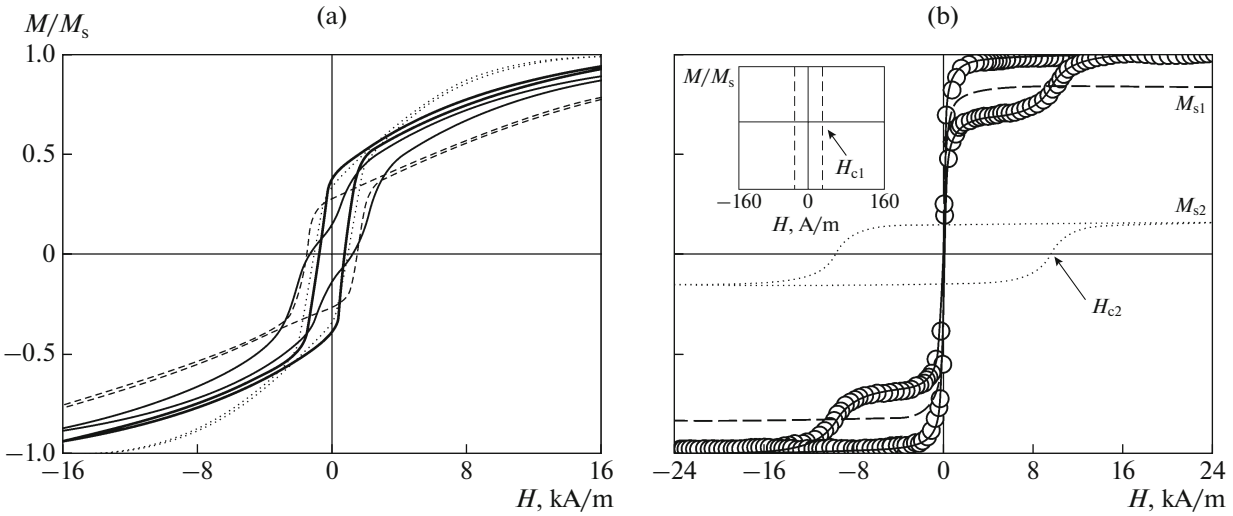

Fig. 5. Hysteresis loops of (a) as-sputtered and (b) annealed (at 500°C) $Fe_{77}Zr_7N_{16}$ films deposited on $Si/SiO_2/Si_3N_4$ substrates and prepared at oblique angles of (a) (bold line) 0°, (dashed line) 10°, (dotted line) 20°, and (thin line) 30° and (b) 20°. Open circles correspond to the experimentally obtained hysteresis loop that is the sum of loops M_{s1} and M_{s2}. (inset) Enlarged area of the origin of coordinates.

likely to indicate the formation of a columnar structure in the films [13], which causes the formation of induced in-plane anisotropy; in this case, the higher the oblique angle, the more substantial the anisotropy (Fig. 5a).

The annealings at 400 and 500°C partly and completely relieve the anisotropy, respectively. The annealings result in a decrease in the coercive force as compared to that for the as-sputtered films; in this case, the higher the oblique angle during sputtering, the more substantial the decrease in the coercive force (Fig. 5b). Moreover, the annealing at 500°C leads to the formation of an additional magnetic anisotropy in the films and a high coercive force (this fact is indicated by widening the hysteresis loop, see Fig. 5b).

The hysteresis loops are described by the empirical function [14]

$$M(H) = M_{s1}(\coth(P_1(H \pm H_{c1})) - (P_1(H \pm H_{c1}))^{-1}) + M_{s2}(\coth(P_2(H \pm H_{c2})) - (P_2(H \pm H_{c2}))^{-1} + \chi H,$$

which allows us to determine the coercive forces (H_{c1}, H_{c2}) in the case of each magnetic anisotropy (see Fig. 5b); depending on the oblique angle and the annealing temperature, these are from 8 to 480 and from 8800 to 14400 A/m, respectively.

Taking into account the prospects to reach a high magnetic permeability of the films at gigahertz frequencies, we calculated the frequency of natural ferromagnetic resonance using the obtained values of H_k and M_s and the expression ${}_e f_{FMR} = \gamma(4\pi M_s H_k)^{1/2}$ (where γ = 2.8 MHz/80 A/m is the gyromagnetic ratio) [1–3, 15]. In this case, the second relatively high magnetic anisotropy (H_{c2} = 13600 A/m) formed in the films (see Fig. 5b) is assumed to give frequency ${}_e f_{FMR}$ up to 4.6 GHz.

CONCLUSIONS

(1) Nanocrystalline $Fe_{77}Zr_7N_{16}$ films with the magnetic anisotropy induced by sputtering at an oblique angle (the angle made by an ion beam with the normal to the substrate surface is 0°, 10°, 20°, and 30°) were studied in the as-sputtered state and after 1-h annealing at 400 and 500°C.

(2) XRD was used to study the effect of the oblique angle during sputtering and the annealing temperature on the phase and structural states of the films. A nanocrystalline phase was found to form in the films. It is the supersaturated nitrogen and zirconium solid solution in bcc α-Fe, which is characterized by a grain size of 2–5 nm and a microstrain of 0.1%. As the oblique angle increases, the lattice parameter of the bcc phase in the as-sputtered films decreases. This indicates a decrease in the nitrogen and zirconium contents in the α-Fe-based solid solution. This is related to the fact that, as the oblique angle increases, the energy conditions of film growth change and, similarly to annealing, affect the structure of the films. The annealings at 400 and 500°C decrease the supersaturation of the bcc solid solution in all films.

(3) The hysteresis loops of the films were measured in fields up to 560 kA/m. The coercive force, the remanent magnetization, the saturation magnetization, and the induced anisotropy field were determined using these hysteresis loops. The induced anisotropy increases up to 3370 ± 30 A/m as the oblique angle increases. During annealing, the induced magnetic anisotropy decreases and, additionally to a coercive force of 24 A/m, a coercive force of 13600 ± 800 A/m is detected, which is related to the second, main magnetic anisotropy.

(4) The perspectives for natural ferromagnetic resonance to be obtained in the films at gigahertz frequencies were estimated.

ACKNOWLEDGMENTS

This study was supported by the Russian Foundation for Basic Research, project no. 15-08-02831a.

REFERENCES

1. S. X. Wang, N. X. Sun, M. Yamaguchi, and S. Yabukami, "Sandwich films: properties of a new soft magnetic material," Nature **407** (6802), 150–151 (2000).
2. I. Kim, J. Kim, K. H. Kim, and M. Yamaguchi, "Effect of boron contents on magnetic properties of Fe–Co–B thin films," IEEE Trans. Magn. **40** (4), 2706–2708 (2004).
3. S. Kong, T. Okamoto, and Sh. Nakagawa, "Improvement of soft magnetic properties of Fe–Co–B underlayer with large saturation magnetization by Ni–Fe–O seedlayers," J. Appl. Phys. **93**, 6778–6780 (2003).
4. E. Yu, J. S. Shim, I. Kim, J. Kim, S. H. Han, H. J. Kim, K. H. Kim, M. Yamaguchi, "Development of FeCo-based thin films for gigahertz applications," IEEE Trans. Magn. **41** (10), 3259–3261 (2005).
5. J. Shim, J. Kim, S. H. Han, H. J. Kim, K. H. Kim, M. Yamaguchi, "Nanocrystalline Fe–Co–Ni–B thin film with high permeability and high-frequency characteristics," J. Magn. Magn. Mater. **290–291**, 205–208 (2005).
6. O. V. Chayka, L. Kraus, F. Fendrych, and S. Veljko, "AC magnetic properties of nanogranular FeCo–AlNi films," Phys. Status Solidi A **204** (6), 1721–1723 (2007).
7. E. N. Sheftel', E. E. Shalygina, G. Sh. Usmanova, S. I. Utitskikh, M. A. Mukasheva, M. Inoue, and R. Fujikawa, "Effect of annealing on the magnetic properties and microstructure of nanocomposite FeZrN films," Pis'ma Zh. Tekhn. Fiz. **33** (20), 64–71 (2007).
8. E. N. Sheftel', "Soft magnetic nanocrystalline Fe–refractory interstitial phase films for magnetic recording application," Materialoved., No. 4, 10–15 (2009).
9. E. N. Sheftel', E. V. Kharin, and S. V. Komogortsev, "Study of the physical nature of the soft magnetic properties of Fe–ZrN nanocrystalline films," Russian Metall., No. 9, 875–881 (2011).
10. E. V. Shelekhov and T. A. Sviridova, "Software for X-ray diffraction analysis of polycrystals," Metalloved. Term. Obrab. Met., No. 8, 16–19 (2000).
11. A. N. Ivanov, E. V. Shelekhov, and E. N. Kuz'mina, "Voigt-function approximation method for determination of nanostructure parameters using X-ray reflection profile," Zavod. Lab. (Diagnostika Mater.) **70** (11), 29–33 (2004).
12. J. Musil, "Hard nanocomposite coatings: thermal stability, oxidation resistance and toughness," Surf. Coating Technol. **207**, 50–65 (2012).
13. S. Tikadzumi, *Physics of Ferromagnetism. Magnetic Characteristics and Applications*, Ed. by R. V. Pisarev (Mir, Moscow, 1987).
14. S. V. Komogortsev, E. A. Denisova, R. S. Iskhakov, A. D. Balaev, L. A. Chekanova, Yu. E. Kalinin, A. V. Sitnikov, "Multilayer nanogranular films $(Co_{40}Fe_{40}B_{20})_{50}(SiO_2)_{50}$/α-Si : H and $(Co_{40}Fe_{40}B_{20})_{50}(SiO_2)_{50}/SiO_2$: magnetic properties," J. Appl. Phys. **113**, 17C105 (2013).
15. I. T. Iakubov, A. N. Lagarkov, S. A. Maklakov, A. V. Osipov, K. N. Rozanov, I. A. Ryzhikov, V. V. Samsonova, A. O. Sboychakov, "Microwave and static magnetic properties of multi-layered iron-based films," J. Magn. Magn. Mater. **321** (7), 726–729 (2009).

Translated by N. Kolchugina